Development of picosecond time-resolved X-ray absorption spectroscopy by high-repetition-rate laser pump/X-ray probe at Beijing Synchrotron Radiation Facility

Hao Wang,[a,b] Can Yu,[a,b] Xu Wei,[a,b] Zhenhua Gao,[a] Guang-Lei Xu,[c] Da-Rui Sun,[a] Zhenjie Li,[a] Yangfan Zhou,[a] Qiu-Ju Li,[a] Bing-Bing Zhang,[a] Jin-Qiang Xu,[c] Lin Wang,[c] Yan Zhang,[a] Ying-Lei Tan[a] and Ye Tao[a]*

[a]Beijing Synchrotron Radiation Facility, Institute of High Energy Physics, Chinese Academy of Sciences, 19B Yuquan Road, Beijing 100049, People's Republic of China, [b]University of Chinese Academy of Sciences, 19B Yuquan Road, Beijing 100049, People's Republic of China, and [c]Accelerator Division, Institute of High Energy Physics, Chinese Academy of Sciences, 19B Yuquan Road, Beijing 100049, People's Republic of China. *Correspondence e-mail: taoy@ihep.ac.cn

A new setup and commissioning of transient X-ray absorption spectroscopy are described, based on the high-repetition-rate laser pump/X-ray probe method, at the 1W2B wiggler beamline at the Beijing Synchrotron Radiation Facility. A high-repetition-rate and high-power laser is incorporated into the setup with in-house-built avalanche photodiodes as detectors. A simple acquisition scheme was applied to obtain laser-on and laser-off signals simultaneously. The capability of picosecond transient X-ray absorption spectroscopy measurement was demonstrated for a photo-induced spin-crossover iron complex in 6 mM solution with 155 kHz repetition rate.

1. Introduction

Picosecond pulses and well defined pulse structure make synchrotrons a desirable light source for time-resolved experiments. Picosecond X-ray time-resolved experiments have been developed based on the pump–probe method, in which a laser pulse first excites a sample and then an X-ray pulse with accurate delay captures the structure of the excited state at that moment. A molecular movie can be obtained if snapshots are taken at different moments during this dynamic process (Chen *et al.*, 2014; Milne *et al.*, 2014; Elsaesser & Woerner, 2010; Kim *et al.*, 2016). The difference between the laser-on and laser-off signals contains dynamic structure information, but it is generally so small that high-quality data are essential for reliable analysis. X-ray absorption spectroscopy can capture the geometrical and electronic structure of the selected atom, such that time-resolved X-ray absorption spectroscopy has been developed over the last few decades at synchrotrons and recently also at X-ray free electron lasers, and this powerful time-resolved probe has been widely applied in diverse fields. Instrumentation and applications of this method have been well reviewed (Chen, 2005; Bressler & Chergui, 2010; Chen *et al.*, 2010, 2014; Milne *et al.*, 2014; Bostedt *et al.*, 2016; Chergui, 2016). The technique of time-resolved X-ray absorption spectroscopy was pioneered at 20 Hz repetition rate with microsecond resolution (Mills *et al.*, 1984) and later realised at 1 kHz repetition rate with pico-second resolution at synchrotrons (Jennings *et al.*, 2002; Saes *et al.*, 2004; Nozawa *et al.*, 2007). At a synchrotron source,
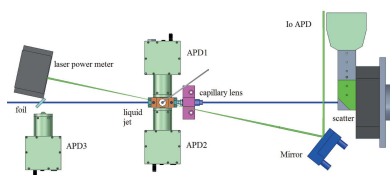
however, the X-ray probe usually comes from a single bunch with repetition rate ranging from several hundreds of kHz to MHz. To obtain high-quality data, it is desirable to match the repetition rate of the laser pulse with that of the X-ray pulse. Therefore, high-repetition-rate pump–probe detection has been developed recently in transient X-ray absorption spectroscopy (Lima *et al.*, 2011; March *et al.*, 2011; Stebel *et al.*, 2011; Göries *et al.*, 2016), emission spectroscopy (Haldrup *et al.*, 2012; Vankó *et al.*, 2013; March *et al.*, 2015), scattering (Haldrup *et al.*, 2012) and diffraction (Navirian *et al.*, 2012; Kozina *et al.*, 2014). To meet the requirements of extremely photon-hungry experiments, like X-ray emission spectroscopy or X-ray solution scattering, some time-resolved experiments have utilized all the X-ray pulses from the storage ring, rather than singlet pulses, with several MHz repetition rate (Haldrup *et al.*, 2012; Vankó *et al.*, 2013; March *et al.*, 2015).

We have built up ultrafast X-ray diffraction detection based on a 1 kHz repetition rate laser pump/X-ray probe scheme at the 1W2B beamline (Sun *et al.*, 2016). However, the low X-ray flux of <1 kHz rate made it extremely difficult to realise the detection of transient X-ray absorption spectroscopy (XAS). Therefore, a high-repetition-rate pump–probe method is essential if we want to obtain transient XAS data with adequate quality within a realistic beam time. In the meantime, it is desirable to improve the data quality of ultrafast X-ray diffraction detection under high repetition rate. Here we describe the setup and commissioning of a high-repetition-rate pump–probe method for detection of transient XAS. Transient XAS has been applied on a photo-induced spin-crossover iron complex to evaluate the performance of the setup.

2. Experimental setup

2.1. X-ray source

The Beijing Synchrotron Radiation Facility (BSRF) is a parasitic light source sharing a storage ring with the Beijing Electron and Positron Collider. In dedicated synchrotron mode the ring energy is 2.5 GeV and the total beam current is 250 mA in top-up mode. The fill frequency is 5 Hz in top-up mode. Hybrid fill pattern mode has become a routine operation with a singlet bunch placed in the gap of bunch trains, as described previously (Sun *et al.*, 2016). The current of the singlet bunch is 2.5 mA at present. The revolution period of the singlet bunch is 804 ns and the repetition rate is 1.243 MHz. The gap between the singlet bunch and the bunch trains is variable; it is 150 ns under current detection. The X-ray pulse duration is around 150 ps.

Beamline 1W2B is a wiggler beamline, and the flux spectrum of the wiggler source is displayed in Fig. 1. The beamline consists of a collimating mirror, a double-crystal fixed-exit Si(111) monochromator and a toroidal mirror. The X-ray energy covers 5–15 keV in practice. The X-ray flux is $\sim 2 \times 10^{10}$ photons s^{-1} at 7 keV at the sample position, corresponding to ~ 160 photons per hybrid pulse. The fluctuation of the hybrid pulse intensity is 0.4% (RMS).

Table 1
Spot size and collection efficiency of the X-ray capillary lens at different X-ray energy.

Energy (keV)	Spot size (μm, FWHM)	Collection efficiency (%)
6	91	32.3
7	90	30.9
10	80	22.3
13	58	13.7
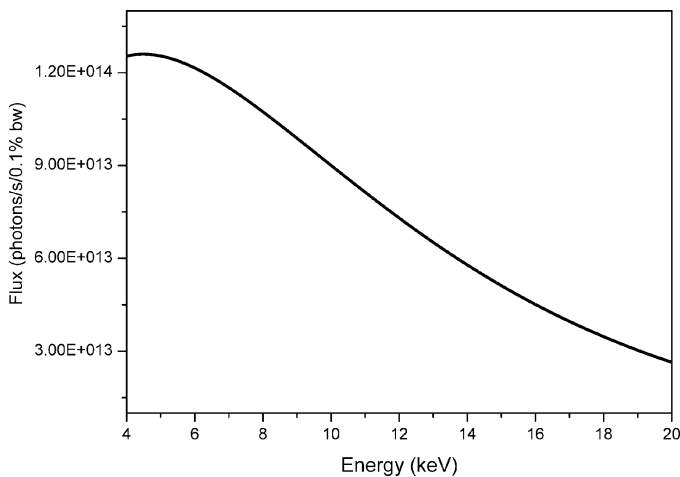
Figure 1
Flux spectrum of the 1W2B wiggler source at 2.5 GeV and 250 mA.

In pump–probe experiments the laser spot size is required to be larger than the X-ray spot size at the sample position to excite the sample throughout. A polycapillary lens focuses the X-rays to 90 μm (FWHM) in two dimensions at 7.2 keV. The spot size and collection efficiency of the capillary lens are summarized for different energies in Table 1. This kind of capillary lens has been used in high-pressure EXAFS detection at the 4W1B wiggler beamline at BSRF (Chen *et al.*, 2013). The laser and X-ray focus sizes were obtained simultaneously by performing knife-edge scans. The stability of the X-ray spot during the energy scan was measured, as shown in Fig. 2. A fluorescence image of the X-ray spot on the scintillator screen was recorded by CCD camera. Then the image was processed to locate the centre position of the X-ray spot. To imitate real X-ray absorption spectroscopy collection, the X-ray energy was continuously scanned over a 900 eV range multiple times during the camera-recording process. The peak-to-peak fluctuation is less than 10% of the X-ray spot size.

2.2. High-repetition-rate laser and synchronization

A high-repetition-rate and high-power fibre laser (Tangerine HP, Amplitude Systems) is installed at the 1W2B beamline. The power of the 1030 nm fundamental is 35 W with a maximum 200 μJ pulse energy. The repetition rate is up to 20 MHz. Parameters of the laser output are summarized in Table 2. The pulse duration is adjustable from 300 fs to 10 ps.
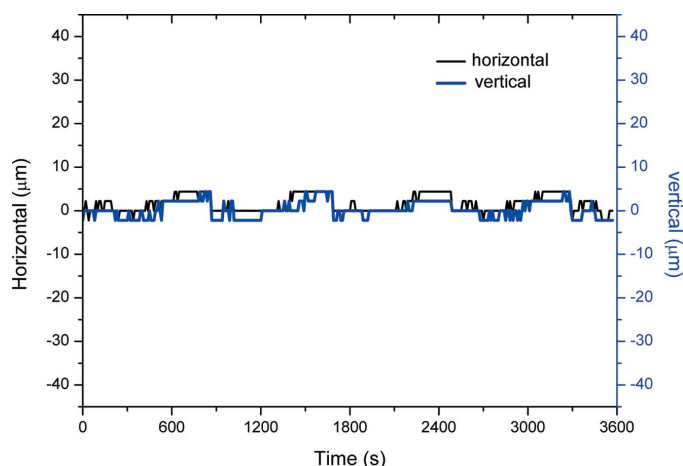
Figure 2
Pointing stability of the focused X-ray spot at the sample position during a large X-ray energy range scan over 1 h.

Table 2
Parameters of laser output at 300 fs pulse duration.

Repetition rate (kHz)	Wavelength (nm)	Power (W)	Pulse energy (μJ)
155	1030	31	200
310	1030	35.2	113.5
620	1030	35	56.5
155	515	13.5	87
310	515	18	58
620	515	15.8	25.5
155	343	6.5	42.1
310	343	11.7	37.7
620	343	9.2	14.8

The second or third harmonic output is often used for experiments. The laser is focused by lenses. The spot size can be adjusted to reach the desirable fluence by changing the focusing lens position along the laser propagation direction. The repetition rate is dependent on the required laser fluence in the experiment.

The synchronization between the X-ray and laser pulse is realised by locking the repetition rate and phase of the oscillator pulse with the storage ring RF signal which has been down divided from 499.8 MHz to 41.65 MHz. Compared with the previous synchronization setup (Sun *et al.*, 2016), the synchronization has been improved, as depicted in Fig. 3. The 500 MHz RF signal is transmitted to the beamline through a clock distribution system (Libera Synch, Instrumentation Technologies), which suppresses the jitter fluctuation in long-distance transmission. The jitter between the RF signal and the laser oscillator signal is less than 500 fs, measured by a signal source analyzer (FSWP8, R&W). The RF signal is input into a programmable delay line (Cobly) before input into the laser oscillator. Fine delay adjustment is made using the programmable delay line with minimum 0.5 ps step and a range of 100 ns. Coarse tuning is realised by selecting different pulses from the oscillator in 24 ns steps, the period of the oscillator pulse.

2.3. Spatial and temporal overlap

Instead of using an X-ray exposure film to determine the spatial overlap, as done previously (Sun *et al.*, 2016), a YAG scintillator crystal screen is used, since the visible fluorescence excited by the X-rays is observable. The fluorescence image of the X-ray focus is observed by microscope. The X-ray position is labelled on a computer, and the spatial overlap can be realised by moving the laser spot to the centre of the labelled area, as shown in the inset of Fig. 4. Then the liquid jet centre is aligned with the position of the surface of the YAG screen to reach the overlap. Fine adjustment is optimized by the sample signal.

After spatial overlap, temporal overlap is achieved by using a fast diode that is sensitive to both X-rays and laser, as shown in Fig. 4. To improve the X-ray signal response, a windowless InGaAs fast photodiode is used with a rise time of 700 ps. The overlap accuracy could be controlled within 200 ps. As with the optimization of the spatial overlap, fine adjustment is optimized by the sample signal.
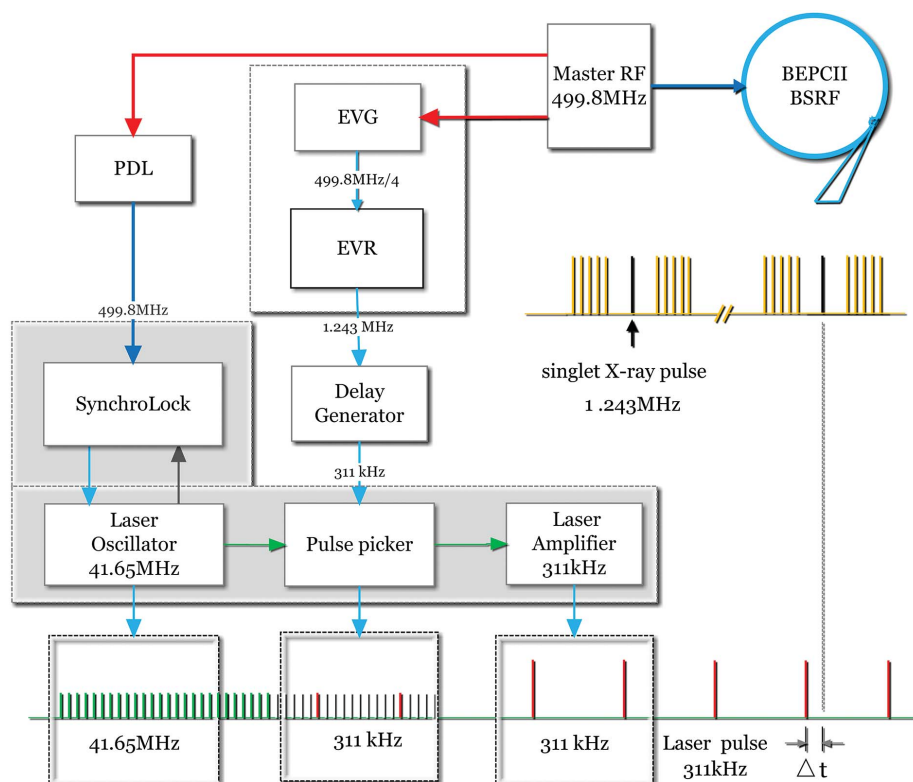
Figure 3
Synchronization layout for the laser-pump/X-ray-probe experiment. The red arrow represents the optic fiber connection. See text for explanation.
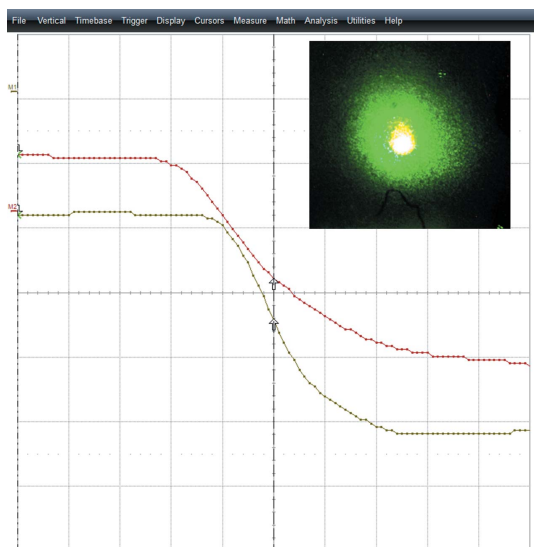
Figure 4
Oscilloscope image of photodiode responses of the X-ray and the laser pulse upon temporal overlap. The upper curve is the X-ray signal (red) and the lower curve the laser signal (green). The cursor line is used as the alignment of two signals at the middle of the rising edges. The display division is 500 ps. The inset shows a spatial overlap image of the X-ray spot (white spot) and the laser spot (green).

2.4. Liquid jet

A liquid jet is essential for transient XAS measurements, since the solution sample needs to be circulated to avoid radiation damage. Fig. 5 shows a liquid jet chamber that was designed to provide a closed room for the sample illuminated by X-ray and laser beams. A sealed chamber is essential for air-sensitive samples. The design enables an avalanche photodiode detector (APD) to be close enough for maximum signal collection. Two 20 µm-thick diamond films are used as
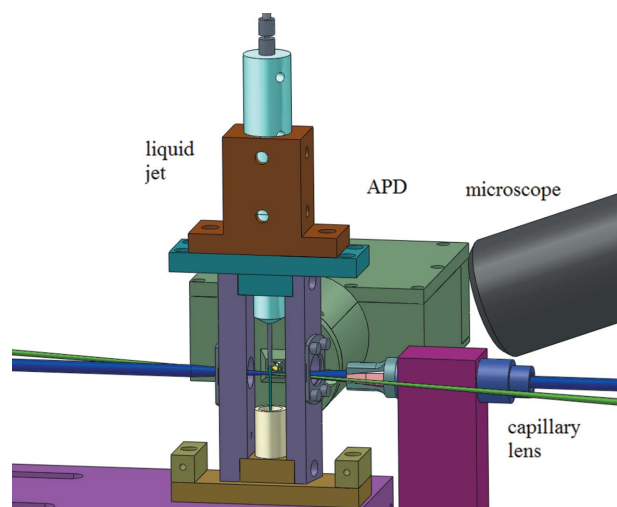
Figure 5
Liquid jet design with an avalanche photodiode detector (APD) installed for the sample signal. The X-ray beam (blue) and laser beam (green) intersect at the liquid jet. A camera with a microscope is used to observe the spatial overlap and monitor the sample under illumination during data collection.

incident and exit window for both X-ray and laser beams. The solution is circulated by a gear pump with a stainless steel tube as nozzle. The inner diameter of the tube is 0.25 mm or 0.5 mm. The liquid flow rate can reach 10 m s^{-1}.

2.5. Detector and Soller slit

We use the fluorescence mode to record the transient X-ray absorption signal. In-house-built APDs are used as detectors, since their nanosecond response is favourable for detection of the signal from the desired bunch. The sensor size is 10 mm × 10 mm with a rise time of ∼2 ns. The detector has a good linearity with count rates up to 8 MHz (Li *et al.*, 2017). The APD sensor is sealed with a beryllium window to block laser scattering. Light-tightness was confirmed with the laser on but X-ray off before collection. As shown in Fig. 6, four APDs are utilized including one for incident (Io APD), two for sample fluorescence (APD 1 and 2) and one for the reference foil as energy calibration (APD3). The Io signal is obtained by detecting the scattering of the X-rays from a thin Mylar film. A laser power meter monitors the laser power stability by measuring the transmitted beam during data collection.

Photocatalysts generally work under low concentrations of less than 10 mM. Therefore, a Soller slit with $Z-1$ filter is needed to block the scattering signal and attenuate fluorescence from the X-ray filter. A cone-shaped Soller slit was designed and manufactured in stainless steel by 3D metal printing. Its transmission efficiency is calculated to be 71.8%. The thickness of the Soller slit is 5.5 mm, and it is calculated that 96% fluorescence from the filter could be blocked. With the Soller slit plus the $Z-1$ filter the silicon drift detector confirmed that the dominant signal came from the $K\alpha$ fluorescence of the sample.

2.6. Data acquisition

The fluorescence signal was estimated to be less than 0.01 photon per X-ray pulse for the model iron complex, so the detection is a single-photon event and we use counting mode to collect the signal. A simple gate scheme is applied to obtain the laser-on and laser-off signals simultaneously. Both laser-on and laser-off gates were generated using digital delay generators (DG645, SRS). The laser-off gate is generated in
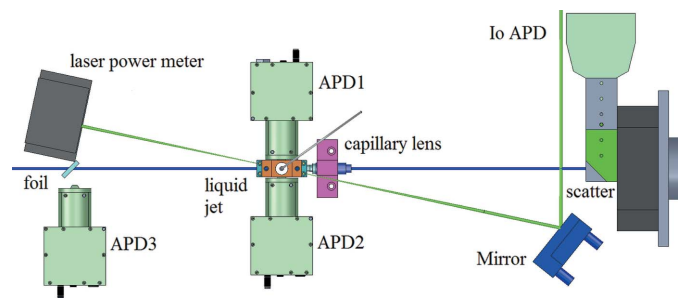
Figure 6
Detection setup for the transient XAS (top view). The laser beam (green) is deflected by a motorized mirror to intersect the X-ray beam (blue) at the sample position.
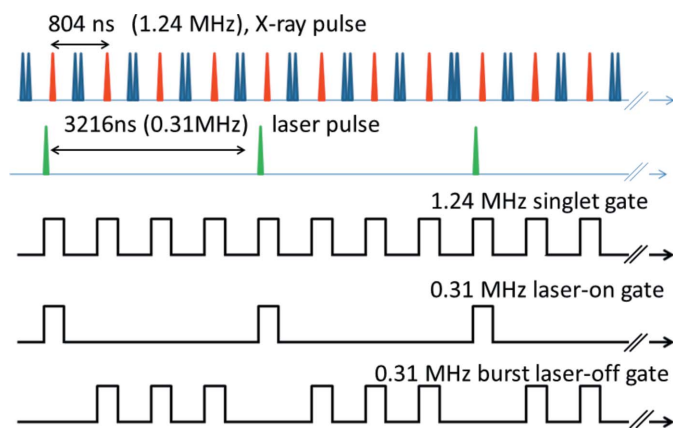
Figure 8
Absorbance of $Fe(II)(phen)_3$, 0.125 mM aqueous solution, path length 5 mm. The inset shows the laser spot on a liquid jet.

burst mode. Fig. 7 shows the gate signal with a laser-on : laser-off ratio of 1:3. The number of delay cycles in the burst (burst count) is three. The gate signals are sent to constant fraction discriminators (CFDs) (CFD 935, ORTEC), which are triggered under gate mode to select the desired laser-on and laser-off signals simultaneously. The output from the CFDs was counted by counters (counter 974, ORTEC). The incident signal and the reference foil signals are gated as well.

3. Commissioning result of picosecond transient XAS

We applied the developed transient XAS on a model iron complex, 1,10-phenanthroline iron(II) sulfate, $Fe(II)(phen)_3$. The iron atom is coordinated to six nitrogen atoms in octahedral configuration, and each phenanthroline ligand provides two nitrogen atoms for coordination. $Fe(II)(phen)_3$ is a low-spin (LS) complex in its ground state, but could be photoexcited to a high-spin (HS) state upon spin crossover. In the relaxation from HS to LS, the lifetime is $\sim$700 ps, which is desirable for a 150 ps X-ray pulse probe. This complex has been well studied using a synchrotron source (Nozawa *et al.*, 2010), so it is a suitable candidate for evaluating the performance of our high-repetition-rate pump–probe setup.

The sample was purchased from Alfa Aesar and used without any further purification. The optical absorption is displayed in Fig. 8. The strongest absorption is at 510 nm, corresponding to a metal-to-ligand charge transfer transition. In the pump–probe experiment, the excitation wavelength is 515 nm. The inset shows an image of a laser spot on the liquid jet. The excitation repetition rate has been tested at 155 and 311 kHz. The 155 kHz mode was selected as it yields the maximum pulse energy of 200 µJ to improve the excitation fraction. The laser pulse duration is 760 fs. A Mn filter with 3 attenuation lengths is used. The flow rate is $\sim$10 m s^{-1} with a nozzle of 0.25 mm inner diameter.

Fig. 9(*a*) displays the transient X-ray absorption near-edge structure (XANES) collected in 3 h. A remarkable difference can be seen between the laser-on and laser-off spectra. In the
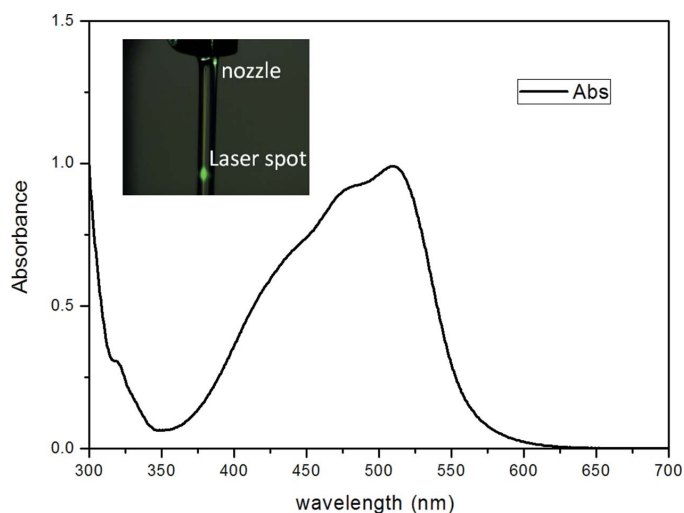
inset, a zoom of the pre-edge region (black arrow) shows the decrease of the magnitude of the pre-edge peak with laser-on. This decrease is direct evidence of the HS excitation state (Nozawa *et al.*, 2010). The laser-on spectrum contains contributions from both ground state and excited state, so the
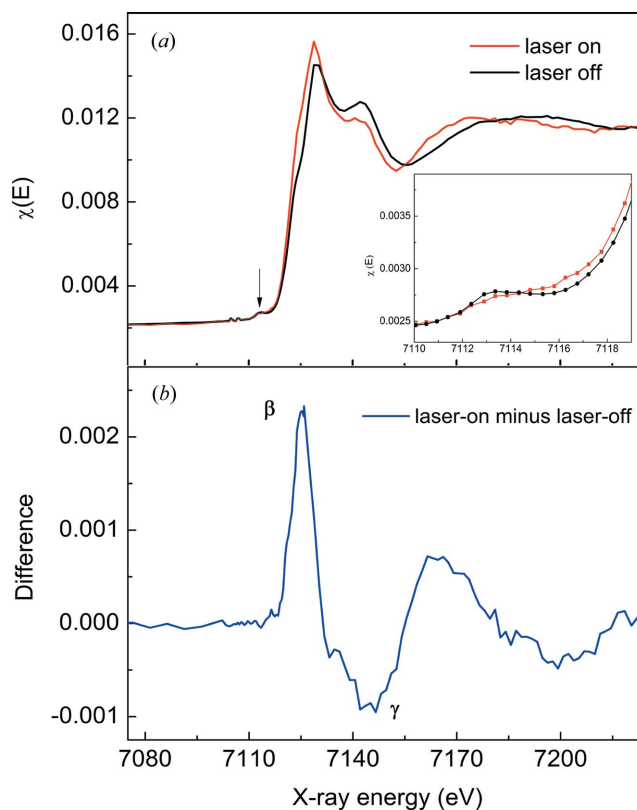
Figure 9
(*a*) Transient XANES of $Fe(II)(phen)_3$ collected at 150 ps after photoexcitation. The excitation wavelength is 515 nm. The sample was dissolved in water and its concentration was 6 mM. The laser fluence was 27 mJ cm^{-2}. The inset shows the pre-edge region scanned at a three times longer collection time for better signal-to-noise ratio. (*b*) Difference spectrum generated from laser-on minus laser-off.
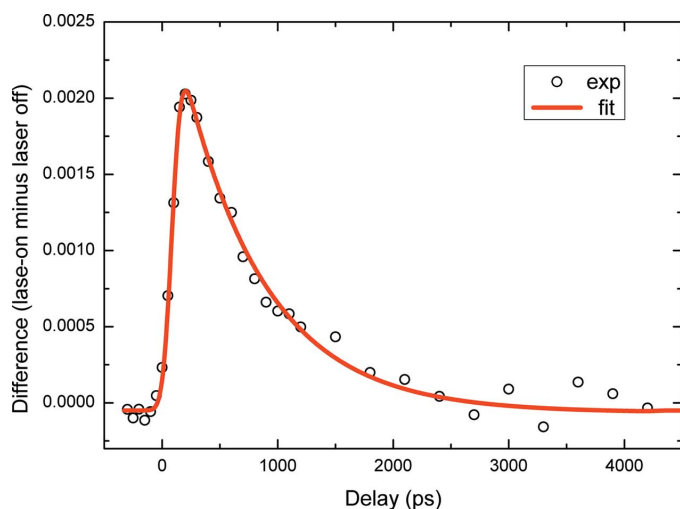
Figure 10
Evolution of the β feature of the difference spectrum (open circles). The solid line is a fit of the convolution of a Gaussian function with a single exponential function.

difference spectrum generated from laser-on minus laser-off can highlight the excited state signal (Fig. 9b). The difference is in agreement with the reported result (Nozawa *et al.*, 2010). The β feature shown in Fig. 9(b) is related to electronic change while the γ feature and the features at higher energy correspond to geometrical structure change.

To evaluate the relaxation process from HS to LS, the X-ray energy is fixed at 7125 eV, *i.e.* the peak position of the β feature. The difference signal at this energy was scanned as a function of the delay between laser pulse and X-ray pulse. As presented in Fig. 10, the evolution data could be fitted with a single exponential function convoluted with a Gaussian function (150 ps FWHM) for the X-ray pulse duration. The lifetime is found to be 685 ps, in agreement with the reported value (Nozawa *et al.*, 2010).

4. Summary and outlook

We have implemented the laser pump/X-ray probe method at high repetition rate. Transient XANES can now be obtained with adequate signal-to-noise ratio within a few hours. Due to low flux, the transient EXAFS measurement will consume a much longer beam time under the current configuration. To improve the detection efficiency, multiple-element APD detectors will help substantially. A linear combination of triple APD sensors with customized electronics is under design. Two combinations are expected to improve the total count rate by a factor of three. Based on the field-programmable gate array technique, a new data acquisition method will enable all bunch signals to be recorded *via* nanosecond time resolution, therefore each bunch signal will be distinguished by its time. Second and third harmonics of the laser are only available for excitation at present. An optical parameter amplifier will soon be installed to realise the excitation range from 210 to 11000 nm.

With the realisation of the transient XAS measurement, a unique X-ray time-resolved platform is in shape at BSRF with the capability of multiple time scale detection from femtoseconds to microseconds. This platform includes both laser plasma table-top X-ray source and synchrotron source. The laser plasma source is superior in the femtosecond X-ray pulse, which enables femtosecond X-ray diffraction (Zhang *et al.*, 2014). Femtosecond X-ray spectroscopy is under planning by utilizing high-energy-resolution superconducting micro-calorimeter spectrometry (Uhlig *et al.*, 2013). The synchrotron has merits in wide tunable X-ray energy, higher pulse intensity stability, high repetition rate and diverse X-ray probes from the picosecond to microsecond range.

References

Bostedt, C., Boutet, S., Fritz, D. M., Huang, Z., Lee, H. J., Lemke, H. T., Robert, A., Schlotter, W. F., Turner, J. J. & Williams, G. J. (2016). *Rev. Mod. Phys.* **88**, 015007.
Bressler, C. & Chergui, M. (2010). *Annu. Rev. Phys. Chem.* **61**, 263–282.
Chen, D. L., Dong, J. C., Zhang, X. L., Quan, P. Y., Liang, Y. X., Hu, T. D., Liu, J., Wu, X., Zhang, Q. & Li, Y. D. (2013). *J. Synchrotron Rad.* **20**, 243–248.
Chen, L. X. (2005). *Annu. Rev. Phys. Chem.* **56**, 221–254.
Chen, L. X., Zhang, X., Lockard, J. V., Stickrath, A. B., Attenkofer, K., Jennings, G. & Liu, D.-J. (2010). *Acta Cryst.* A**66**, 240–251.
Chen, L. X., Zhang, X. & Shelby, M. L. (2014). *Chem. Sci.* **5**, 4136–4152.
Chergui, M. (2016). *Struct. Dynam.* **3**, 031001.
Elsaesser, T. & Woerner, M. (2010). *Acta Cryst.* A**66**, 168–178.
Göries, D., Dicke, B., Roedig, P., Stübe, N., Meyer, J., Galler, A., Gawelda, W., Britz, A., Gessler, P., Sotoudi Namin, H., Beckmann, A., Schlie, M., Warmer, M., Naumova, M., Bressler, C., Rübhausen, M., Weckert, E. & Meents, A. (2016). *Rev. Sci. Instrum.* **87**, 053116.
Haldrup, K., Vankó, G., Gawelda, W., Galler, A., Doumy, G., March, A. M., Kanter, E. P., Bordage, A., Dohn, A., van Driel, T. B., Kjaer, K. S., Lemke, H. T., Canton, S. E., Uhlig, J., Sundström, V., Young, L., Southworth, S. H., Nielsen, M. M. & Bressler, C. (2012). *J. Phys. Chem. A*, **116**, 9878–9887.
Jennings, G., Jäger, W. J. H. & Chen, L. X. (2002). *Rev. Sci. Instrum.* **73**, 362–368.
Kim, J., Kim, K. H., Oang, K. Y., Lee, J. H., Hong, K., Cho, H., Huse, N., Schoenlein, R. W., Kim, T. K. & Ihee, H. (2016). *Chem. Commun.* **52**, 3734–3749.
Kozina, M., Hu, T., Wittenberg, J. S., Szilagyi, E., Trigo, M., Miller, T. A., Uher, C., Damodaran, A., Martin, L., Mehta, A., Corbett, J., Safranek, J., Reis, D. A. & Lindenberg, A. M. (2014). *Struct. Dynam.* **1**, 034301.

Li, Z., Li, Q., Jinfan, C., Ma, Y., Liu, P., Wang, Z., Hu, M. Y., Zhao, J., Alp, E. E., Xu, W., Tao, Y., Wu, C. & Zhou, Y. (2017). *Nucl. Instrum. Methods Phys. Res. A.* Submitted.

Lima, F. A., Milne, C. J., Amarasinghe, D. C. V., Rittmann-Frank, M. H., van der Veen, R. M., Reinhard, M., Pham, V. T., Karlsson, S., Johnson, S. L., Grolimund, D., Borca, C., Huthwelker, T., Janousch, M., van Mourik, F., Abela, R. & Chergui, M. (2011). *Rev. Sci. Instrum.* **82**, 063111.

March, A. M., Assefa, T. A., Bressler, C., Doumy, G., Galler, A., Gawelda, W., Kanter, E. P., Németh, Z., Pápai, M., Southworth, S. H., Young, L. & Vankó, G. (2015). *J. Phys. Chem. C*, **119**, 14571–14578.

March, A. M., Stickrath, A., Doumy, G., Kanter, E. P., Krässig, B., Southworth, S. H., Attenkofer, K., Kurtz, C. A., Chen, L. X. & Young, L. (2011). *Rev. Sci. Instrum.* **82**, 073110.

Mills, D. M., Lewis, A., Harootunian, A., Huang, J. & Smith, B. (1984). *Science*, **223**, 811–813.

Milne, C. J., Penfold, T. J. & Chergui, M. (2014). *Coord. Chem. Rev.* **277–278**, 44–68.

Navirian, H., Shayduk, R., Leitenberger, W., Goldshteyn, J., Gaal, P. & Bargheer, M. (2012). *Rev. Sci. Instrum.* **83**, 063303.

Nozawa, S., Adachi, S., Takahashi, J., Tazaki, R., Guérin, L., Daimon, M., Tomita, A., Sato, T., Chollet, M., Collet, E., Cailleau, H., Yamamoto, S., Tsuchiya, K., Shioya, T., Sasaki, H., Mori, T., Ichiyanagi, K., Sawa, H., Kawata, H. & Koshihara, S. (2007). *J. Synchrotron Rad.* **14**, 313–319.

Nozawa, S., Sato, T., Chollet, M., Ichiyanagi, K., Tomita, A., Fujii, H., Adachi, S. & Koshihara, S. (2010). *J. Am. Chem. Soc.* **132**, 61–63.

Saes, M., van Mourik, F., Gawelda, W., Kaiser, M., Chergui, M., Bressler, C., Grolimund, D., Abela, R., Glover, T. E., Heimann, P. A., Schoenlein, R. W., Johnson, S. L., Lindenberg, A. M. & Falcone, R. W. (2004). *Rev. Sci. Instrum.* **75**, 24–30.

Stebel, L., Malvestuto, M., Capogrosso, V., Sigalotti, P., Ressel, B., Bondino, F., Magnano, E., Cautero, G. & Parmigiani, F. (2011). *Rev. Sci. Instrum.* **82**, 123109.

Sun, D.-R., Xu, G.-L., Zhang, B.-B., Du, X.-Y., Wang, H., Li, Q.-J., Zhou, Y.-F., Li, Z.-J., Zhang, Y., He, J., Yue, J.-H., Lei, G. & Tao, Y. (2016). *J. Synchrotron Rad.* **23**, 830–835.

Uhlig, J., Fullagar, W., Ullom, J. N., Doriese, W. B., Fowler, J. W., Swetz, D. S., Gador, N., Canton, S. E., Kinnunen, K., Maasilta, I. J., Reintsema, C. D., Bennett, D. A., Vale, L. R., Hilton, G. C., Irwin, K. D., Schmidt, D. R. & Sundström, V. (2013). *Phys. Rev. Lett.* **110**, 138302.

Vankó, G., Bordage, A., Glatzel, P., Gallo, E., Rovezzi, M., Gawelda, W., Galler, A., Bressler, C., Doumy, G., March, A. M., Kanter, E. P., Young, L., Southworth, S. H., Canton, S. E., Uhlig, J., Smolentsev, G., Sundström, V., Haldrup, K., van Driel, T. B., Nielsen, M. M., Kjaer, K. S. & Lemke, H. T. (2013). *J. Electron Spectrosc. Relat. Phenom.* **188**, 166–171.

Zhang, B. B., Sun, S. S., Sun, D. R. & Tao, Y. (2014). *Rev. Sci. Instrum.* **85**, 096110.